CROATICA CHEMICA ACTA
CCACAA **76** (3) 189–197 (2003)

ISSN-0011-1643
CCA-2871
Original Scientific Paper

A Model of CE Mechanism on Spherical Electrodes

Milivoj Lovrić[a,*] and Yakov I. Tur'yan[b]

[a]*Center for Marine and Environmental Research, Ruđer Bošković Institute, P.O. Box 180, Zagreb 10002, Croatia*

[b]*The National Physical Laboratory of Israel, Danciger »A« Bldg, Givat Ram, 91904 Jerusalem, Israel*

RECEIVED OCTOBER 23, 2002; REVISED JANUARY 27, 2003; ACCEPTED FEBRUARY 5, 2003

Key words
CE mechanism
chronoamperometry
spherical electrodes
microelectrodes

A model of electrode reaction preceded by a first-order chemical reaction under chronoamperometric conditions on spherical electrodes has been developed. A general solution applying to all values of equilibrium constants, including very small ones, was obtained by numerical integration. Well-known analytical solutions for steady-state and near-steady-state conditions and for pure kinetic currents were shown to be special cases of the general solution. The conditions for their application are given.

INTRODUCTION

Kinetics of some homogeneous chemical reactions can be measured by electrochemical methods because the chemical disbalance can be maintained at the electrode surface by the electro-consumption of one of the components of the system[1]. This is called a CE mechanism.[2] Some examples of the preceding reactions are the dissociation of metal complexes,[3,4] the dehydration of carbonyl compounds,[5–7] or the deprotonation of acids.[8] The theory of CE mechanism was developed for various electrochemical methods, such as chronoamperometry,[3,8–11] polarography,[5,12–14] pulse polarography,[15] cyclic voltammetry,[1,16] rotating disk[2] and square-wave voltammetry,[17,18] using a stationary planar,[9,18] a stationary spherical,[3,8,10,11,17] expanding plane,[12,13] expanding sphere[14,15] and cylindrical[16] diffusion models under the steady-state,[3,8–12,14] or transient conditions.[13,15–18] The steady-state models are based on the assumption that the difference between the equilibrium concentrations and the actual concentrations of electroinactive and electroactive forms of the reactant is independent of time. This condition is satisfied if the ratio of concentrations of electroinactive and electroactive forms is very high in the equilibrium. In that case, the current depends entirely on the rate of the preceding reaction. If this rate tends to zero, the current vanishes. However, if the equilibrium ratio of concentrations of two forms of the reactant is rather small, the diffusion of electroactive form from the bulk of the solution towards the electrode surface contributes significantly to the current. Thus, the current does not vanish even if the rate of the preceding reaction is reduced to zero. This observation can be explained only by general models, in which no steady-state approximations are applied.[6]

In this communication, a general solution for chronoamperometry of CE mechanism on spherical electrodes is developed in order to estimate the conditions under which the steady-state assumption[3,8,10,11] is justified. The model applies to static mercury drop electrodes (r_0 = 0.3 mm)[19] and hemispherical semimicro- (r_0 = 60 μm)[20] and microelectrodes (r_0 = 5 μm)[21].

* Author to whom correspondence should be addressed. (E-mail: mlovric@rudjer.irb.hr)

THE MODEL

An electrode reaction under a high overvoltage, preceded by a first-order chemical reaction, is considered:

$$Z \underset{kK}{\overset{k}{\leftrightarrow}} Ox \xrightarrow{+ne^-} \text{product} \tag{1}$$

where k is the chemical reaction rate constant, $K = c_Z^*/c_{Ox}^*$ is the equilibrium constant and c_Z^* and c_{Ox}^* are bulk concentrations of the species Z and Ox, respectively. A big difference between the electrode potential and the standard potential of the redox reaction is assumed, so that the influence of electrode kinetics can be neglected. At spherical electrodes, reaction (1) can be described by the system of differential equations:

$$\frac{\partial(rc_{Ox})}{\partial t} = D\frac{\partial^2(rc_{Ox})}{\partial r^2} + kr(c_Z - Kc_{Ox}) \tag{2}$$

$$\frac{\partial(rc_Z)}{\partial t} = D\frac{\partial^2(rc_Z)}{\partial r^2} - kr(c_Z - Kc_{Ox}) \tag{3}$$

with the initial and boundary conditions:

$$t = 0,\ r \geq r_0: \quad c_{Ox} = c_{Ox}^*,\ c_Z = c_Z^* \tag{4}$$

$$t > 0,\ r \to \infty: \quad c_{Ox} \to c_{Ox}^*,\ c_Z \to c_Z^* \tag{5}$$

$$r = r_0: \quad c_{Ox,r=r_0} = 0 \tag{6}$$

$$(\partial c_Z / \partial r)_{r=r_0} = 0 \tag{7}$$

$$(\partial c_{Ox} / \partial r)_{r=r_0} = I / nFSD \tag{8}$$

Here, D is the common diffusion coefficient, r_0 is the electrode radius, S is the electrode surface area and I is the current. Eqs. (2) and (3) were derived using the relationship:

$$D\left(\frac{\partial^2 c}{\partial r^2} + \frac{2}{r}\cdot\frac{\partial c}{\partial r}\right) = \frac{D}{r}\cdot\frac{\partial^2(rc)}{\partial r^2} \tag{9}$$

Eqs. (2) and (3) are solved using the well known substitutions:[12]

$$\psi = c_{Ox} + c_Z \tag{10}$$

$$\omega = c_Z - K c_{Ox} \tag{11}$$

Thus, the new system of equations is obtained:

$$\frac{\partial(r\psi)}{\partial t} = D\frac{\partial^2(r\psi)}{\partial r^2} \tag{12}$$

$$\frac{\partial(r\omega)}{\partial t} = D\frac{\partial^2(r\omega)}{\partial r^2} - k(1+K)(r\omega) \tag{13}$$

$$t = 0,\ r \geq r_0: \quad \psi = c_{Ox}^* + c_Z^*,\ \omega = 0 \tag{14}$$

$$t > 0,\ r \to \infty: \quad \psi \to c_{Ox}^* + c_Z^*,\ \omega \to 0 \tag{15}$$

$$r = r_0: \quad \psi_{r=r_0} = \omega_{r=r_0} \tag{16}$$

$$(\partial\psi / \partial r)_{r=r_0} = I / nFSD \tag{17}$$

$$(\partial\omega / \partial r)_{r=r_0} = -KI / nFSD \tag{18}$$

As shown in Appendix I, its solution is an integral equation:[22]

$$c_{Ox}^*(1+K) - \int_0^t \frac{I}{nFS\sqrt{D}}\left[\frac{1}{\sqrt{\pi(t-\tau)}} - a\cdot e^{a^2(t-\tau)}\cdot\mathrm{erfc}(a\sqrt{t-\tau})\right]d\tau = K\int_0^t \frac{I}{nFS\sqrt{D}}\cdot e^{-\varepsilon(t-\tau)}\cdot\left[\frac{1}{\sqrt{\pi(t-\tau)}} - a\cdot e^{a^2(t-\tau)}\cdot\mathrm{erfc}(a\sqrt{t-\tau})\right]d\tau \tag{19}$$

where $\varepsilon = k(1+K)$ and $a = \sqrt{D} / r_0$.

For the purpose of numerical integration, Eq. (19) is transformed into the system of recursive formulae:

$$\Phi_1 = \frac{\left(\frac{\rho^2}{K} - K\kappa^2\right)\sqrt{\pi}}{R_1\rho - P_1 K\kappa + \left(\frac{\rho}{K} - \frac{K\kappa^2}{\rho}\right)Q_1}$$

$$\Phi_m = \frac{\left(\frac{\rho^2}{K} - K\kappa^2\right)\sqrt{\pi} - \sum_{j=1}^{m-1}\Phi_j\left[R_{m-j+1}\rho - P_{m-j+1}K\kappa + Q_{m-j+1}\left(\frac{\rho}{K} - \frac{K\kappa^2}{\rho}\right)\right]}{R_1\rho - P_1 K\kappa + \left(\frac{\rho}{K} - \frac{K\kappa^2}{\rho}\right)Q_1} \tag{20}$$

where:

$$\Phi = I\sqrt{t\pi} / nFSc_{Ox}^*(1+K)\sqrt{D}$$

$$\kappa = \sqrt{kt(1+K)} / K$$

$$\rho = \sqrt{Dt} / r_0$$

$$P_1 = \mathrm{erf}\,(K\kappa / 10)$$

$$P_i = \text{erf}\,(K\kappa\sqrt{i}\,/\,10) - \text{erf}\,(K\kappa\sqrt{i-1}\,/\,10)$$

$$Q_1 = 1 - \exp(\rho^2/100)\cdot\text{erfc}(\rho/10)$$

$$Q_i = \exp\left[\rho^2\,(i-1)/100\right]\cdot\text{erfc}(\rho\sqrt{i-1}\,/\,10) - \exp\left[\rho^2\,i/100\right]\cdot\text{erfc}(\rho\sqrt{i}\,/\,10)$$

$$R_1 = 1 - \exp\left[(\rho^2 - K^2\kappa^2)/100\right]\cdot\text{erfc}(\rho/10)$$

$$R_i = \exp\left[(\rho^2 - K^2\kappa^2)\,(i-1)/100\right]\cdot\text{erfc}(\rho\sqrt{i-1}\,/\,10) - \exp\left[(\rho^2 - K^2\kappa^2)\,i/100\right]\cdot\text{erfc}(\rho\sqrt{i}\,/\,10)$$

and $100 \geq m \geq 1$. Eq. (20) applies to $D / r_0^2 \neq k\,(1+K)$.

A Special Solution for $\partial\omega / \partial t = 0$

$$\Phi_{\partial\omega/\partial t = 0} = f\left[\rho\sqrt{\pi} + f\cdot F(z)\right] \tag{21}$$

where:

$$f = \frac{K\kappa + \rho}{K\kappa + \rho(1+K)}$$

$$F(z) = z\sqrt{\pi}\cdot\exp(z^2)\cdot\text{erfc}(z)$$

$$z = \kappa + \rho\,(1+K)/K$$

Eq. (21) is identical with Eq. (24) in the paper of Budevskii and Desimirov.[11]

A Special Solution for $\partial\psi / \partial t = 0$

$$I_{\partial\psi/\partial t = 0} = \frac{nFSc^*_{\text{Ox}}(1+K)D}{r_0}\cdot\frac{K\kappa + \rho}{K\kappa + \rho(1+K)} \tag{22}$$

Eq. (22) is identical with Oldham's equation (25).[10] Note that from $\partial\omega / \partial t = 0$ it follows that $\partial c_Z / \partial t = K\cdot\partial c_{\text{Ox}} / \partial t$, but $\partial\psi / \partial t \neq 0$. However, if $\partial\psi / \partial t = 0$, then $\partial c_{\text{Ox}} / \partial t = 0$ and $\partial c_Z / \partial t = 0$, and so $\partial\omega / \partial t = 0$. Equation (21) corresponds to the kinetic steady-state approximation used in the planar diffusion models, while equation (22) describes the steady-state diffusion conditions at microelectrodes.

RESULTS AND DISCUSSION

The electrode mechanism (1) is characterized by two trivial limiting conditions. If $K \to 0$, the bulk concentration of the species Z also tends to zero and the dimensionless current Φ tends to the limiting value:

$$\Phi_{\text{lim}} = 1 + \rho\sqrt{\pi} \tag{23}$$

If $\kappa \to 0$, the rate of the preceding chemical reaction is negligible and the current depends only on the bulk concentration of the species Ox:

$$\lim_{\kappa\to 0}\Phi = (1 + \rho\sqrt{\pi})\,/\,(1+K) \tag{24}$$

If $\kappa \to \infty$, the preceding reaction is so fast that the equilibrium between the species Z and Ox is permanently maintained both in the bulk of the solution and in the diffusion layer. So, the dimensionless current tends to the limiting value:

$$\lim_{\kappa\to\infty}\Phi = \Phi_{\text{lim}} \tag{25}$$

Mathematically, this condition corresponds to the special solution $\omega = 0$. Function ω depends on the chemical disbalance in the solution.

Finally, if $K \to \infty$, the concentration c^*_{Ox} is negligible and the current depends entirely on the rate of decomposition of the Z species. It is sometimes called a pure kinetic current.[6] Considering Eqs. (24) and (25), two limiting values of the pure kinetic current can be noticed:

$$\lim_{K\to\infty}\left(\lim_{\kappa\to 0}\Phi\right) = 0 \tag{26}$$

$$\lim_{K\to\infty}\left(\lim_{\kappa\to\infty}\Phi\right) = \Phi_{\text{lim}} \tag{27}$$

The dimensionless current Φ depends on the dimensionless kinetic parameter $\kappa = \sqrt{kt(1+K)}\,/\,K$, the dimensionless sphericity parameter $\rho = \sqrt{Dt}\,/\,r_0$ and the equilibrium constant K. The pure kinetic current ($K >> 1$) is independent of the equilibrium constant. Variation of the measurement time changes both parameters, κ and ρ, but not their ratio. If $\rho \to 0$, the solutions of the spherical and planar diffusion models are identical. The latter solution is given in Appendix I.

Figure 1 shows the dependence of the ratio of the kinetic and limiting currents $I / I_{\text{lim}} = \Phi / \Phi_{\text{lim}}$, where Φ_{lim} is defined by Eq. (23), on the kinetic parameter κ, for various equilibrium constants K and the sphericity parameters ρ. The chosen values of the latter parameter (ρ = 0.1, 1 and 10) correspond to 10 seconds of electrolysis at a constant and high overvoltage on spherical or hemispherical electrodes with radii r_0 = 1 mm, 100 μm and 10 μm, respectively, all assuming that $D = 10^{-5}$ cm^2 s^{-1}. If the equilibrium constant is small, the ratio I / I_{lim} is a sigmoidal curve increasing with κ from $(1 + K)^{-1}$ to 1. If $K > 10^2$, this relationship is a parabolic curve. On spherical macro-electrodes ($\rho = 0.1$), the dependence of I / I_{lim} on κ is essentially similar to the corresponding relationship on planar electrodes, as can be seen by comparing Figures 1A and 2. On microelectrodes (ρ = 1 and 10), the increasing of I / I_{lim} with κ is significantly slower than on macro-electrodes. If $K \geq 10^2$, this ratio is lower

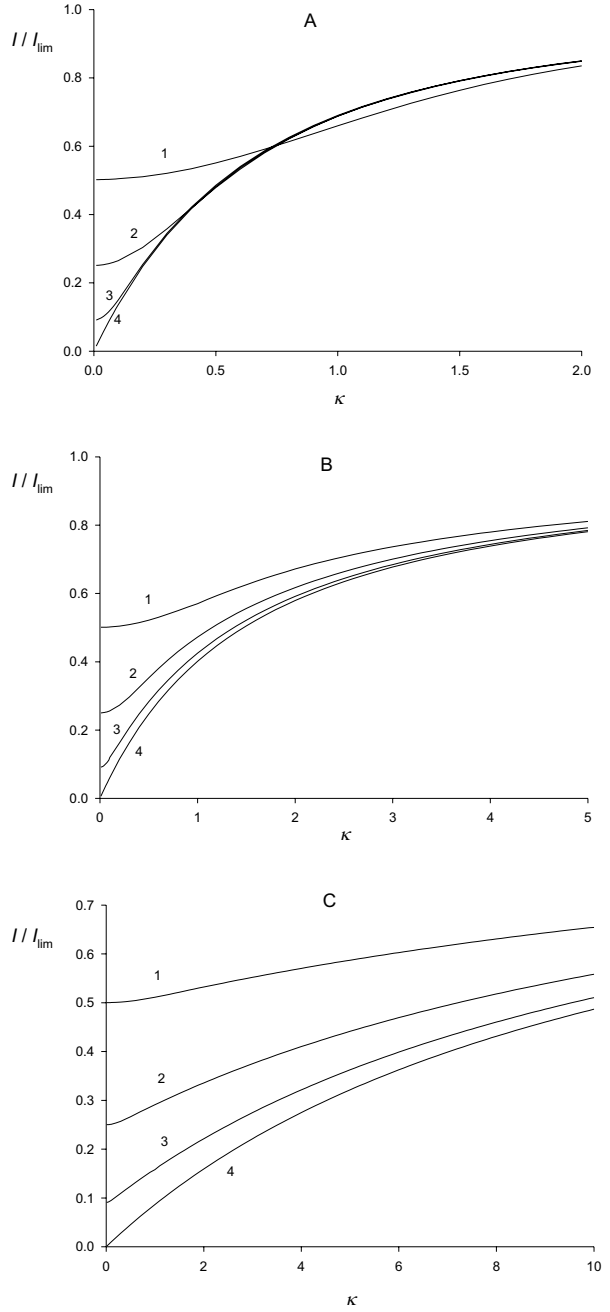

Figure 1. Dependence of the ratio of kinetic (Eq. 20) and limiting (Eq. 23) currents on parameter κ, for ρ = 0.1 (A), 1 (B) and 10 (C). K = 1 (1), 3 (2), 10 (3) and 10^4 (4).

than 0.9 if κ is smaller than 2.6, 12 and 94, for ρ = 0.1, 1 and 10, respectively. This means that for the same κ and K values the preceding chemical reaction appears slower on microelectrodes than on macro-electrodes. Hence, faster reactions can be measured on microelectrodes.

The influence of the measurement duration on the ratio I / I_{lim} is shown in Figure 3. The increasing of time is expressed as the increasing of the kinetic parameter κ, but the ratio ρ / κ is constant. In Figure 3 this ratio is very high: $\rho = 10\kappa$, which corresponds to the conditions on microelectrodes. Compared to Figure 1C, the ratio

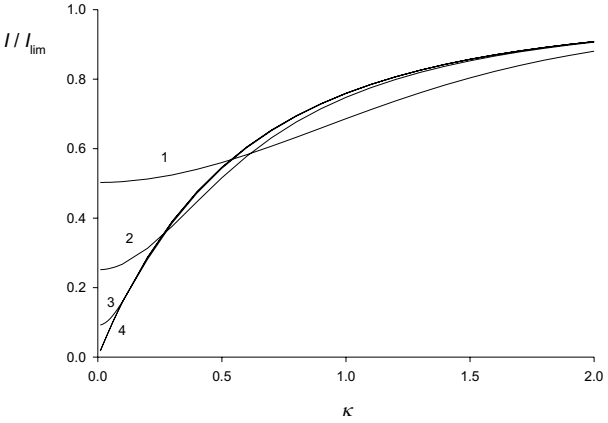

Figure 2. Relationship between I / I_{lim} and κ on the planar electrode (Eq. A9). K = 1 (1), 3 (2), 10 (3) and 10^4 (4).

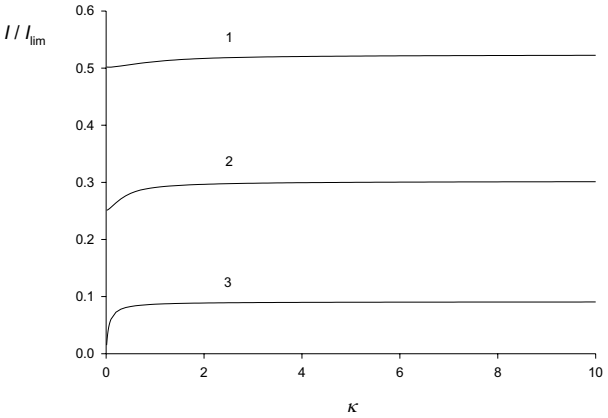

Figure 3. Dependence of I / I_{lim} on κ, for the constant ratio ρ/κ = 10. K = 1 (1), 3 (2) and 10^4 (3).

TABLE I. Dependence of the ratio I / I_{lim} on the kinetic parameter κ and the equilibrium constant K. The planar diffusion model (Eq. A9)

κ	I / I_{lim}			
K:	1	3	10	>100
0.2	0.512	0.313	0.281	0.287
0.4	0.540	0.447	0.473	0.476
0.6	0.582	0.578	0.603	0.604
0.8	0.633	0.677	0.694	0.694
1.0	0.686	0.748	0.759	0.759
1.2	0.737	0.799	0.807	0.807
1.4	0.783	0.837	0.843	0.843
1.6	0.822	0.866	0.870	0.870
1.8	0.855	0.889	0.891	0.891
2.0	0.880	0.906	0.908	0.908
2.5	0.924	0.937	0.937	0.937
3.0	0.948	0.955	0.956	0.956

I / I_{lim} does not increase to 1, but towards a lower boundary that depends on the equilibrium constant. These boundaries are: 0.52 (K = 1), 0.30 (K = 3) and 0.091 (K = 10^4).

TABLE II. Dependence of the ratio I / I_{lim} on the kinetic parameter κ, for various measurement times. The static mercury drop electrode: $r_0 = 0.3$ mm, $D = 10^{-5}$ cm^2 s^{-1}

(A) $K = 1$

κ	I / I_{lim}					
t / s:	5	10	20	30	60	120
0.5	0.524	0.538	0.533	0.530	0.525	0.520
1.0	0.634	0.620	0.605	0.596	0.580	0.565
1.5	0.725	0.703	0.680	0.665	0.640	0.616
2.0	0.790	0.765	0.737	0.720	0.689	0.659
2.5	0.833	0.808	0.778	0.760	0.727	0.694
3.0	0.862	0.837	0.808	0.790	0.757	0.722
3.5	0.882	0.859	0.831	0.813	0.780	0.745
4.0	0.898	0.876	0.849	0.832	0.800	0.765
4.5	0.910	0.889	0.864	0.847	0.816	0.782
5.0	0.919	0.890	0.876	0.860	0.830	0.797
6.0	0.934	0.916	0.894	0.880	0.852	0.821
7.0	0.944	0.928	0.908	0.895	0.869	0.840
8.0	0.951	0.937	0.919	0.907	0.883	0.855
9.0	0.957	0.944	0.928	0.916	0.894	0.868
10.0	0.962	0.950	0.935	0.924	0.903	0.878
11.0	0.966	0.955	0.940	0.931	0.911	0.888
12.0	0.969	0.959	0.945	0.936	0.918	0.895
13.0	0.972	0.962	0.949	0.941	0.923	0.902
14.0	0.974	0.965	0.953	0.945	0.928	0.908
15.0	0.976	0.967	0.956	0.948	0.933	0.914
16.0	0.978	0.969	0.959	0.951	0.937	0.918
18.0	0.981	0.973	0.964	0.957	0.943	0.926
20.0	0.983	0.976	0.967	0.961	0.949	0.933

(B) $K = 100$

κ	I / I_{lim}					
t / s:	5	10	20	30	60	120
0.5	0.419	0.384	0.345	0.320	0.277	0.233
1.0	0.615	0.573	0.525	0.494	0.438	0.379
1.5	0.721	0.681	0.633	0.601	0.543	0.480
2.0	0.785	0.748	0.703	0.673	0.616	0.554
2.5	0.827	0.793	0.751	0.724	0.670	0.609
3.0	0.856	0.825	0.787	0.761	0.711	0.653
3.5	0.877	0.849	0.814	0.790	0.743	0.688
4.0	0.894	0.867	0.835	0.813	0.769	0.717
4.5	0.906	0.882	0.852	0.831	0.790	0.741
5.0	0.916	0.894	0.866	0.846	0.807	0.761
6.0	0.931	0.912	0.887	0.870	0.835	0.793
7.0	0.942	0.925	0.903	0.887	0.856	0.818
8.0	0.950	0.934	0.915	0.901	0.872	0.837
9.0	0.956	0.942	0.924	0.911	0.885	0.853
10.0	0.961	0.948	0.932	0.920	0.896	0.866
11.0	0.965	0.953	0.938	0.927	0.905	0.877
12.0	0.968	0.957	0.943	0.933	0.912	0.886
13.0	0.971	0.961	0.948	0.938	0.919	0.894
14.0	0.974	0.964	0.951	0.943	0.924	0.901
15.0	0.976	0.966	0.955	0.947	0.929	0.907
16.0	0.977	0.969	0.958	0.950	0.934	0.913
18.0	0.980	0.973	0.963	0.956	0.941	0.922
20.0	0.983	0.976	0.967	0.960	0.947	0.929

If the ratio ρ / κ is 0.1 and 1, the relationships between I / I_{lim} and κ are qualitatively similar to those shown in Figures 1A and 1B, respectively, and the maximum values of the ratio I / I_{lim} are: 0.92 ($K = 1$) and 0.91 ($K = 10^4$) if $\rho / \kappa = 0.1$, and 0.57 ($K = 3$), 0.52 ($K = 10$) and 0.50 ($K = 10^4$) if $\rho / \kappa = 1$.

Tables I, II and III show the theoretical relationships between the ratio I / I_{lim} and the kinetic parameter κ, for various equilibrium constants K and three types of electrodes: a large stationary disk, a small static mercury drop and two hemispherical microelectrodes. These tables can be used to estimate the rate constant k from the experimental data if constant K is known. The main difference between the planar and spherical electrodes appears when the measurement time is varied. There is a family of curves on the spherical electrode, which all correspond to the same equilibrium constant K, but to measurements of different duration, because of the change of the apparent electrode sphericity with the change of the measurement time. The data in Table II cover the sphericity parameters from $\rho = 0.236$ ($t = 5$ s) to $\rho = 1.155$ ($t = 120$ s). Precision of the rate constant determination depends on the gradient $\partial(I / I_{lim}) / \partial\kappa$. If $K > 100$ and the planar electrode is used, good results can be obtained if $I / I_{lim} < 0.9$, or $\kappa < 2$. If $K = 1$, this condition is $0.5 < \kappa < 2.5$. On the mercury drop electrode, the condition changes from $\kappa < 5$, for $t = 5$ s, to $\kappa < 10$ for $t = 120$ s. On microelectrodes, the ratio I / I_{lim}

TABLE III. Dependence of the ratio I / I_{lim} on the kinetic parameter κ, for two measurement times. Hemispherical microelectrodes: $r_0 = 60$ μm and 25 μm; $K = 100$ and $D = 10^{-5}$ cm^2 s^{-1}

κ	I / I_{lim}		κ	I / I_{lim}	
	$r_0 = 60$ μm			$r_0 = 25$ μm	
	$t = 10$ s	$t = 60$ s		$t = 10$ s	$t = 60$ s
1	0.317	0.183	2	0.310	0.168
2	0.482	0.306	4	0.471	0.284
3	0.584	0.397	6	0.572	0.371
4	0.653	0.467	8	0.640	0.439
5	0.702	0.522	10	0.690	0.494
6	0.739	0.567	12	0.728	0.539
7	0.768	0.605	14	0.757	0.577
8	0.792	0.636	16	0.781	0.609
9	0.811	0.663	18	0.800	0.636
10	0.826	0.686	20	0.817	0.660
12	0.851	0.724	24	0.842	0.700
14	0.870	0.754	30	0.870	0.744
16	0.885	0.778	34	0.884	0.767
18	0.896	0.797	40	0.899	0.795
20	0.906	0.814	44	0.908	0.810
25	0.924	0.845	50	0.918	0.829
30	0.936	0.868	60	0.931	0.853
35	0.945	0.885	70	0.940	0.872
40	0.951	0.898	80	0.947	0.886
45	0.957	0.908	90	0.953	0.897
50	0.961	0.916	100	0.957	0.907

may appear almost independent of the measurement time. This can be seen in Table III. If for r_0 = 25 μm and t = 10 s (ρ = 4.0), κ = 10 and $I / I_{\lim}$ = 0.690, then for t = 60 s (ρ = 9.8) κ = 24.5 but $I / I_{\lim}$ = 0.704. Also, if for t = 10 s, κ = 30 and $I / I_{\lim}$ = 0.870, then for t = 60 s, κ = 73.5 but $I / I_{\lim}$ = 0.875.

The described results can be partly explained by analyzing the approximative equation (21), which is calculated assuming that $\partial\omega / \partial t = 0$. It is demonstrated in Appendix II that the result obtained in this way satisfies the initial assumption, within an error of 1 %, if $\kappa + \rho(1+K) / K > 4$. Equation (21) is characterized by the following limiting values: $\lim_{\rho\to 0} \Phi_{\partial\omega/\partial t=0} = F(\kappa)$ (see Eq. A10 in Appendix I), $\lim_{\kappa\to\infty} \Phi_{\partial\omega/\partial t=0} = \lim_{K\to 0} \Phi_{\partial\omega/\partial t=0} = 1 + \rho\sqrt{\pi} = \Phi_{\lim}$ (see Eqs. 23 and 25), $\lim_{K\to\infty} \Phi_{\partial\omega/\partial t=0} = \kappa\left[\rho\sqrt{\pi} + \kappa F(\kappa+\rho) / (\kappa+\rho)\right] / (\kappa+\rho)$ and $\lim_{\kappa\to 0}(\lim_{K\to\infty} \Phi_{\partial\omega/\partial t=0}) = 0$ and $\lim_{\kappa\to\infty}(\lim_{K\to\infty} \Phi_{\partial\omega/\partial t=0}) = \Phi_{\lim}$, which is in agreement with Eqs. (26) and (27). However, the limiting value $\lim_{\kappa\to 0} \Phi_{\partial\omega/\partial t=0} = \left[\rho\sqrt{\pi} + F(\rho(1+K) / K) / (1+K)\right] / (1+K)$ is in disagreement with Eq. (24), except for $K \to \infty$. Thus, the approximative equation (21) should differ from the general solution if both κ and K are small. This can be seen from Figure 4. Curves 1–3 and 4–6 are calculated using Eqs. (20) and (21), respectively. Figure 4A (ρ = 0.1) can be compared with Figure 2. The curve calculated using Eq. (A10) is identical with curve 4 in Figure 2. If K = 1, the result of Eq. (A10) is accurate if $\kappa > 3.5$ and if K = 3 the limit of accuracy is $\kappa > 1.5$, but if $K > 10^2$ the result is accurate in the whole range of κ values. The same conditions apply to spherical macro-electrodes, as can be seen by comparing curves 1 and 4, as well as curves 2 and 5 in Figure 4A. Equation (21) describes the pure kinetic current accurately (see curves 3 and 6). On microelectrodes, the accuracy of Eq. (21) increases proportionally to the value of parameter ρ (see Figures 4B and 4C). In the first approximation, the gradient $\partial(I / I_{\lim}) / \partial\kappa$ of the pure kinetic current ($\lim_{K\to\infty} \Phi_{\partial\omega/\partial t=0}$) is close to the ratio $\kappa / (\kappa + \rho)$ and decreases as ρ is increasing.

If the ratio ρ / κ is constant $\rho = w\,\kappa$, as in the case of the measurement time variation, equation (21) can be transformed as follows:

$$\Phi_{\partial\omega/\partial t=0} / \Phi_{\lim} = f_1\left[w\kappa\sqrt{\pi} + f_1 F(z_1)\right] / (1 + w\kappa\sqrt{\pi}) \quad (28)$$

where:

$$f_1 = \frac{1+\dfrac{w}{K}}{1+w\dfrac{1+K}{K}}$$

$$z_1 = \kappa\left(1+w\frac{1+K}{K}\right)$$

The ratio $I / I_{\lim}$ estimated using Eq. (28) exhibits two limiting values: $\lim_{\kappa\to 0}(\Phi_{\partial\omega/\partial t=0} / \Phi_{\lim}) = 0$ and $\lim_{\kappa\to\infty}(\Phi_{\partial\omega/\partial t=0} / \Phi_{\lim}) = f_1$. The limit for $\kappa \to \infty$ is smaller than 1 for any $w > 0$. This is shown in Figure 5, for ρ / κ = 10. Curves

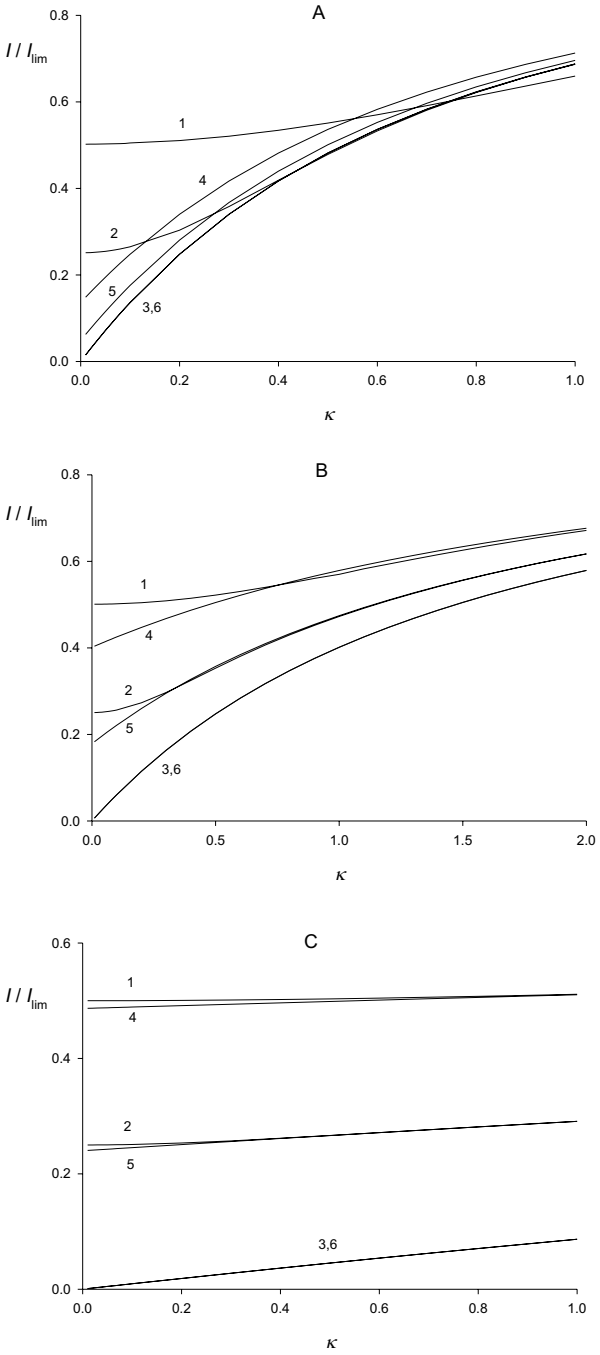

Figure 4. Comparison of the ratio $I / I_{\lim}$ calculated by Eq. (20) (curves 1–3) and Eq. (21) (curves 4–6), for ρ = 0.1 (A), 1 (B) and 10 (C). K = 1 (1 and 4), 3 (2 and 5) and 10^4 (3 and 6).

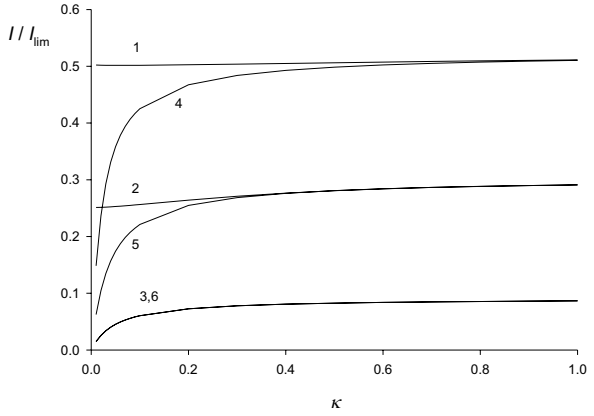

Figure 5. Comparison of the ratio I / I_{lim} calculated by Eq. (20) (curves 1–3) and Eq. (21) (curves 4–6), for the constant ratio $\rho/\kappa = 10$. $K = 1$ (1 and 4), 3 (2 and 5) and 10^4 (3 and 6).

1–3 are calculated by Eq. (20) and curves 4–6 by Eq. (28). The approximative and general solutions are equal if $\rho > 10$, for $K = 1$, and $\rho > 4$, for $K = 3$. There is no restriction for pure kinetic current (see curves 3 and 6). Curves 1–3 are the same as those shown in Figure 3. Their limiting values for $\kappa \to \infty$ are equal to factor f_1. The same boundary value of equation (21) can be obtained by considering the limiting value of the real current when the measurement time is increased to infinity:

$$I_{\partial\omega/\partial t=0} = nFSC^*_{Ox}(1+K)\sqrt{D}f\left[\frac{\sqrt{D}}{r_0} + \frac{f}{\sqrt{t\pi}}F(z)\right] \quad (29)$$

$$\lim_{t\to\infty}(I_{\partial\omega/\partial t=0} / I_{lim}) = \frac{\sqrt{k(1+K)} + \sqrt{D}/r_0}{\sqrt{k(1+K)} + \sqrt{D}(1+K)/r_0} \quad (30)$$

where: $I_{lim} = nFSc^*_{Ox}(1 + K)D / r_0$. Equation (30) is identical to equation (22) and Oldham's equation (25),[10] as well as to the limiting value of equation (28) for $t \to \infty$. Note that $\rho / \kappa = K\sqrt{D} / r_0\sqrt{k(1+K)}$. The calculations show that Eq. (28) approaches Eq. (30) if $\rho > 50$. This is in agreement with the condition $\rho > 100/\sqrt{\pi}$. Hence, Oldham's equation can be used if this condition is satisfied. If the rate constant k is measured using microelectrodes with various radii, the minimal measurement times that satisfy the condition for the steady-state $\partial\psi / \partial t = 0$ are: $t = 63$ s (for $r_0 = 5$ μm), $t = 250$ s ($r_0 = 10$ μm), $t = 1563$ s ($r_0 = 25$ μm) and $t = 6250$ s ($r_0 = 50$ μm). Obviously, at some microelectrodes, the measurements can be performed only under near-steady-state conditions.

For the pure kinetic current ($K > 100$) under the steady-state conditions ($\rho > 50$), Eq. (30) can be simplified if $w_{K>100} / K << 1$, where: $w_{K>100} = \sqrt{DK} / r_0\sqrt{k}$. Under this condition one obtains:

$$(I_{\partial\psi/\partial t=0} / I_{lim})_{K>100} = \frac{1}{1 + w_{K>100}} \quad (31)$$

and

$$\sqrt{\frac{k}{K}} = \frac{\sqrt{D}}{r_0} \cdot \frac{(I_{\partial\psi/\partial t=0} / I_{lim})_{K>100}}{1 - (I_{\partial\psi/\partial t=0} / I_{lim})_{K>100}} \quad (32)$$

In conclusion, the rate constant k can be determined using Eqs. (30), or (32) if $\rho > 50$. If $\rho < 50$, but $K > 100$, Eqs. (21) and (28) can be used. If $\rho < 50$ and $K < 100$, Eq. (20) must be used. On planar electrodes, Eq. (A10) can be used if $K > 100$, and Eq. (A9) if $K < 100$. For some particular cases, the data in Tables I–III can be used.

Calculations of rate constants of the dehydration of several carbonyl compounds were reported in our previous paper.[6] Here, the application of the theory is explained by analyzing an imaginary experiment. The rate constant of the preceding chemical reaction can be determined if the equilibrium constant of the electroinactive and electroactive forms of reactant (K), as well as their average diffusion coefficient (D), are known. It is assumed that the two-electron electrode reaction of the species Z and Ox is measured at constant potential on the static mercury drop electrode of radius $r_0 = 0.3$ mm (see equation 1). It is further assumed that $K = 100$, $D = 10^{-5}$ cm^2 s^{-1} and $c^*_{Ox} + c^*_Z = 10^{-3}$ mol L^{-1}, as well as that the currents measured after 5, 10, 20 and 30 seconds are 1.9, 1.6, 1.3 and 1.2 μA, respectively. The limiting currents at these times are calculated by the following equation:

$$I_{lim} = nFS(c^*_{Ox} + c^*_Z)\left(\sqrt{\frac{D}{t\cdot\pi}} + \frac{D}{r_0}\right) \quad (33)$$

So, the limiting currents and the corresponding ratios of the kinetic and limiting currents are: 2.47, 1.96, 1.60 and 1.44 μA, and 0.77, 0.82, 0.81 and 0.83, for $t = 5$, 10, 20 and 30 seconds, respectively. Using the first four columns of Table II (for $K = 100$), it can be seen that the calculated ratios I / I_{lim} correspond to the following values of the dimensionless kinetic parameters κ: 1.9, 2.9, 3.5 and 4.5. The rate constants are calculated using the equation:

$$k = \frac{\kappa^2 \cdot K^2}{t\cdot(1+K)} \quad (34)$$

The results are: 71.5, 83.3, 60.6 and 66.8 s^{-1}. Hence, the average value of the rate constant of the preceding chemical reaction is $\bar{k} = 70 \pm 10$ s^{-1}. This procedure shows that for each CE mechanism, specific relationships between I / I_{lim} and κ, for particular values of K, D, r_0 and t, have to be calculated using Eq. (20).

APPENDIX I

A General Solution

Using the Laplace transforms, differential equations (12) and (13) are solved in the Laplace space:

$$L\psi_{r=r_0} = \frac{c^*_{Ox} + c^*_Z}{s} - \frac{1}{\sqrt{s}+a} \cdot L\frac{I}{nFS\sqrt{D}} \quad \text{(A1)}$$

$$L\omega_{r=r_0} = \frac{K}{\sqrt{s+\varepsilon}+a} \cdot L\frac{I}{nFS\sqrt{D}} \quad \text{(A2)}$$

where s is a transformation variable, while a and ε are defined after Eq. (19). Considering equation (16), the inverse Laplace transformation of Eqs. (A1) and (A2) results in equation (19).

For the numerical integration, the following transformations were used:

$$LJ_1 = \frac{1}{s} \cdot \frac{1}{\sqrt{s+\varepsilon}+a} \quad \text{(A3)}$$

$$s + \varepsilon = s^* \quad \text{(A4)}$$

$$LJ_1 = \frac{1}{a^2-\varepsilon} \cdot \frac{a^2-\varepsilon}{(s^*-\varepsilon)(\sqrt{s^*}+a)} \quad \text{(A5)}$$

They are correct if $a^2 \neq \varepsilon$.

A Steady-state Approximation: $\partial\omega / \partial t = 0$

Under this condition, the solution of equation (13) is:

$$\omega_{r=r_0} = \frac{K}{a+\sqrt{\varepsilon}} \cdot \frac{I}{nFS\sqrt{D}} \quad \text{(A6)}$$

Because of equation (16), the Laplace transformation of Eq. (A6) is combined with Eq. (A1):

$$\frac{c^*_{Ox} + c^*_Z}{s} = \left(\frac{1}{\sqrt{s}+a} + \frac{K}{a+\sqrt{\varepsilon}}\right) \cdot L\frac{I}{nFS\sqrt{D}} \quad \text{(A7)}$$

Equation (21) is obtained by the inverse Laplace transformation of Eq. (A7).

A Steady-state Diffusion Model: $\partial\psi / \partial t = 0$

The solution of equation (12) is:

$$\psi_{r=r_0} = c^*_{Ox} + c^*_Z - \frac{1}{a} \cdot \frac{I}{nFS\sqrt{D}} \quad \text{(A8)}$$

Equation (22) is obtained by combining Eqs. (16), (A6) and (A8).

A General Solution for the Planar Diffusion Model

$$\Phi_{1,\text{planar}} = \frac{1}{\frac{1}{5\pi} + \frac{P_1}{\kappa\sqrt{\pi}}}$$

$$\Phi_{m,\text{planar}} = \frac{1 - \sum_{j=1}^{m-1} \Phi_{j,\text{planar}} \left(\frac{U_{m-j+1}}{5\pi} + \frac{P_{m-j+1}}{\kappa\sqrt{\pi}}\right)}{\frac{1}{5\pi} + \frac{P_1}{\kappa\sqrt{\pi}}} \quad \text{(A9)}$$

where: $U_1 = 1$, $U_i = \sqrt{i} - \sqrt{i-1}$, while κ, Φ and P_i are defined after Eq. (20).

A Special Solution for $\partial\omega / \partial t = 0$

$$\Phi_{\text{planar},\partial\omega / \partial t = 0} = F(\kappa) \quad \text{(A10)}$$

where: $F(\kappa) = \kappa\sqrt{\pi} \cdot \exp(\kappa^2) \cdot \text{erfc}(\kappa)$.

The well known Eq. (A10)[2] is characterized by the following limiting values:

$$\lim_{\kappa\to 0} F(\kappa) = 0 \quad \text{and} \quad \lim_{\kappa\to\infty} F(\kappa) = 1.$$

APPENDIX II

The Condition that Justifies the Assumption that $\partial\omega / \partial t = 0$

If it is assumed that $\partial\omega / \partial t = 0$, the solution of Eq. (13) is equation (A6), and the solution of Eqs. (12) and (13) is:[11]

$$\frac{I}{nFSc^*_{Ox}(1+K)\sqrt{D}} = \frac{a+\sqrt{\varepsilon}}{K} \cdot \left[p + q \cdot e^{u^2 t} \cdot \text{erfc}(u\sqrt{t})\right] \quad \text{(A11)}$$

where:

$$u = \frac{\sqrt{\varepsilon}}{K} + a\frac{1+K}{K}$$

$$p = \frac{aK}{a(1+K)+\sqrt{\varepsilon}}$$

$$q = \frac{a+\sqrt{\varepsilon}}{a(1+K)+\sqrt{\varepsilon}}$$

Hence, the first derivative on t of Eq. (A6) is:

$$\frac{\partial\omega_{r=r_0}}{\partial t} = qc^*_{Ox}(1+K)\frac{\partial}{\partial t} e^{u^2 t} \text{erfc}(u\sqrt{t}) \quad \text{(A12)}$$

The solution of Eq. (A12) is:

$$\frac{\partial\omega_{r=r_0}}{\partial t} = \frac{qc^*_{Ox}(1+K)u}{\sqrt{t\pi}} \left[u\sqrt{t\pi} \cdot e^{u^2 t} \text{erfc}(u\sqrt{t}) - 1\right] \quad \text{(A13)}$$

Considering Eq. (A10), the assumption $\partial\omega / \partial t = 0$ is satisfied only if $u\sqrt{t} \to \infty$. However, an approximative condition, with the error of 1 %, can be postulated:

$$F(u\sqrt{t}) \geq 1 - 0.01 \cdot u\sqrt{t} \qquad \text{(A14)}$$

which is satisfied for

$$u\sqrt{t} \geq 4 \qquad \text{(A15)}$$

REFERENCES

1. F. Marken, A. Neudeck, and A. M. Bond, in: F. Scholz (Ed.), *Electroanalytical Methods*, Springer, Berlin, 2002, pp. 85–86.
2. A. J. Bard and L. R. Faulkner, *Electrochemical Methods*, John Wiley & Sons, New York, 2001, pp. 492–495.
3. J. Galceran, J. Puy, J. Salvador, J. Cecilia, and H. P. van Leeuwen, *J. Electroanal. Chem*. **505** (2001) 85–94.
4. H. P. van Leeuwen and J. P. Pinheiro, *J. Electroanal. Chem*. **471** (1999) 55–61.
5. Y. I. Tur'yan, *Croat. Chem. Acta* **72** (1999) 13–24.
6. Y. I. Tur'yan and M. Lovrić, *J. Electroanal. Chem*. **531** (2002) 147–154.
7. R. Rodriguez-Amaro, E. Muñoz, J. J. Ruiz, J. L. Avila, and L. Camacho, *Electrochim. Acta* **39** (1994) 107–113.
8. M. Fleischmann, F. Lasserre, J. Robinson, and D. Swan, *J. Electroanal. Chem*. **177** (1984) 97–114.
9. J. Koutecký and R. Brdička, *Collect. Czech. Chem. Commun*. **12** (1947) 337–341.
10. K. B. Oldham, *J. Electroanal. Chem*. **313** (1991) 3–16.
11. E. Budevskii and G. Desimirov, *Dokladi Akad. Nauk SSSR* **149** (1963) 120–123.
12. J. Koutecký, *Collect. Czech. Chem. Commun*. **18** (1953) 597–610.
13. C. Nishihara and H. Matsuda, *J. Electroanal. Chem*. **73** (1976) 261–266.
14. J. Koutecký and J. Čižek, *Collect. Czech. Chem. Commun*. **21** (1956) 836–843.
15. A. A. A. M. Brinkman and J. M. Los, *J. Electroanal. Chem*. **14** (1967) 269–284.
16. J. A. Alden, F. Hutchinson, and R. G. Compton, *J. Phys. Chem. B* **101** (1997) 949–958.
17. A. Molina, C. Serna, and F. Martinez-Ortiz, *J. Electroanal. Chem*. **486** (2000) 9–15.
18. A. B. Miles and R. G. Compton, *J. Electroanal. Chem*. **499** (2001) 1–16.
19. W. A. Peterson, *Am. Lab*. **11** (1979) 69–72.
20. J. Golas, Z. Galus, and J. Osteryoung, *Anal. Chem*. **59** (1987) 389–392.
21. S. P. Kounaves and W. Deng, *Anal. Chem*. **65** (1993) 375–377.
22. Š. Komorsky-Lovrić, M. Lovrić and A. M. Bond, *Electroanalysis* **5** (1993) 29–40.

SAŽETAK

Model CE mehanizma na sferičnim elektrodama

Milivoj Lovrić i Yakov I. Tur'yan

Razvijen je matematički model elektrodne reakcije kojoj prethodi kemijska reakcija prvog reda za kronoamperometriju na sferičnim elektrodama. Numeričkom integracijom dobiveno je opće rješenje koje vrijedi za sve vrijednosti konstanti ravnoteže elektroinaktivnoga i elektroaktivnoga oblika reaktanta. Pokazano je da su poznata analitička rješenja za čistu kinetičku struju i za struju koja ne ovisi o vremenu posebni slučajevi općega rješenja. Određeni su uvjeti za njihovu primjenu.